Finite-temperature properties of the relaxor $PbMg_{1/3}Nb_{2/3}O_3$ from atomistic simulations

A. Al-Barakaty,[1] Sergey Prosandeev,[2,*] Dawei Wang,[3] B. Dkhil,[4] and L. Bellaiche[2]

[1]*Physics Department, Jamoum University College, Umm Al-Qura University, Makkah, Makkah 21955, Saudi Arabia*

[2]*Physics Department and Institute for Nanoscience and Engineering, University of Arkansas, Fayetteville, Arkansas 72701, USA*

[3]*Electronic Materials Research Laboratory, Key Laboratory of the Ministry of Education and International Center for Dielectric Research, Xi'an Jiaotong University, Xi'an 710049, China*

[4]*Laboratoire Structures, Propriétés et Modélisation des Solides, CentraleSupélec, Université Paris-Saclay, CNRS-UMR8580, Grande Voie des Vignes, 92295 Châtenay-Malabry Cedex, France*

(Received 27 February 2015; published 30 June 2015)

An atomistic numerical scheme is developed and used to study the prototype of relaxor ferroelectrics, that is $PbMg_{1/3}Nb_{2/3}O_3$ (PMN), at finite temperatures. This scheme not only reproduces known complex macroscopic properties of PMN, but also provides a deep microscopic insight into this puzzling system. In particular, relaxor properties of PMN are found to originate from the competition between (1) random electric fields arising from the alloying of Mg and Nb ions belonging to different columns of the Periodic Table within the same sublattice; (2) the simultaneous condensation of *several* off-center **k** points as a result of a specific short-range, antiferroelectriclike interaction between lead-centered dipoles; and (3) ferroelectriclike interactions. Such origins contrast with those recently proposed for the homovalent $Ba(Zr,Ti)O_3$ solid solution, despite the fact that these two materials have similar macroscopic properties—which therefore leads to a comprehensive understanding of relaxor ferroelectrics.

DOI: 10.1103/PhysRevB.91.214117 PACS number(s): 77.80.Jk, 77.22.Ch, 77.22.Ej

I. INTRODUCTION

Relaxor ferroelectrics have attracted much attention since their discoveries more than five decades ago. In particular, numerous studies have been conducted on the prototype of ferroelectric relaxors, that is lead magnesium niobate $PbMg_{1/3}Nb_{2/3}O_3$ (PMN), and have revealed anomalous features, which are also inherent to some magnetic systems [1,2] therefore extending their significance beyond ferroelectrics. For instance, PMN adopts a dielectric response-versus-temperature function that possesses a rounded peak, having a large magnitude and is strongly dependent on the frequency of the applied ac electric field, while PMN remains *macroscopically* nonpolar, down to the lowest temperatures [3,4]. Measurements of its inverse dielectric permittivity [5] as a function of temperature have also revealed an unusual deviation from linear behavior for a specific temperature, which is now known as the Burns temperature T_B [6].

Several conflicting models have been proposed to understand the microscopic origin of relaxor ferroelectrics, in general, and of PMN, in particular. A popular belief to explain their macroscopic anomalies is the existence of the so-called polar nanoregions (PNRs) [5–9]. These polar correlations are thought to appear at T_B and to freeze on cooling, as similar to the dipole glass state. Another widespread and alternative model is that PMN owes its unusual properties to the development of a state formed by nanoscale multidomains [10–13]. Indeed, Ref. [12] proposed that quenched random fields (arising from the fact that the randomly distributed Mg and Nb cations possess different nominal ionic charges) prevent the normal ferroelectric state to take place and rather break it down into a nanodomains state. Reference [10] suggested that the large magnitude of the dielectric permittivity of PMN is then due to the side-wall motion in these nanodomains. Actually, the glassy-state versus nanodomains model is still debated and no consensus or satisfactory description of the real structure currently exists. As detailed in some reviews [3,13–15], other concepts have also been considered to explain the peculiar properties of PMN, including chemically ordered regions [16] possessing large dielectric response [17,18], overbonded oxygen ions [19], polaronic mechanism [20,21], and the coexistence of ferroelectric and antiferroelectric couplings [22]. It is also unclear if the recent mechanism that has been determined from first-principles-based calculations on the homovalent $Ba(Zr,Ti)O_3$ (BZT) relaxor ferroelectric—that is the coexistence within the same material of ferroelectrically active and ferroelectrically inactive (silent) ions [23]—holds for PMN.

A comprehensive understanding of lead-based relaxors, in general, and its representative compound, i.e., PMN, in particular, is therefore still lacking, despite the introduction of remarkable pioneering analytical approaches, such as the random-site [24], spherical-random-bond-random-field [25], and soft pseudospin glass [26] models as well as other models [27]. One reason behind this paucity of knowledge is that finite-temperature properties of heterovalent lead-based relaxors are rather challenging to mimic due, e.g., to the facts that its mixed B sublattice is formed by ions that are chemically very different (Mg and Nb in PMN) and that the other cation sublattice possesses (lead) ions that strongly desire to move away from their ideal positions [7,28,29].

The goal of this paper is to report the development and results of an atomistic numerical scheme that is able to realistically mimic the subtle and intriguing features of PMN, and which further provides a deep insight (that we believe to be unprecedented) into the microscopic description of this prototypical relaxor ferroelectric. In particular, this scheme reveals the major importance of random electric fields as well as complex and unexpected antiferroelectriclike interactions

*sprossan@uark.edu

(involving *several* off-center vectors in the reciprocal space), allowing us to understand the properties of PMN. The use of this scheme also resolves the aforementioned issues about the microscopic nature of PMN, and also elucidates the (controversial) effect of chemical ordering on properties of PMN.

II. METHODS

As detailed in the Supplemental Material [30–35], we developed an effective Hamiltonian (H_{eff}) for PMN. Its degrees of freedom are as follows: (1) The local soft-mode in unit cell i, $\mathbf{u}_i$, which represents the collective motion of Pb, Mg/Nb, and oxygen ions associated with the lowest transverse optical phonon branch [36]. $\mathbf{u}_i$ is therefore directly proportional to the local electric dipole moment in cell i. It is technically chosen to be centered on the Pb sites, as consistent with the known fact that lead ions significantly move of center in Pb-based perovskites [28,29,37–40]; (2) Nb/Mg-centered dimensionless local displacements $\mathbf{v}_i$ that are related to the inhomogeneous strain inside each cell [36]; (3) The homogeneous strain tensor, η_H [36]. Such effective Hamiltonian also depends on $\{\sigma_j\}$ variables that characterize the atomic configuration of the PMN solid solution. More precisely, $\sigma_j = +1$ or -1 corresponds to the presence of a Mg or Nb atom located at the B-lattice site j, respectively [41]. Here, we average properties over 30 different alloy configurations, all randomly selected and frozen during the simulations, in order to mimic well disordered PMN systems [42]. Monte Carlo simulations using this H_{eff} are performed using $18 \times 18 \times 18$ supercells (29 160 atoms) with periodic boundary conditions. Note that the parameters entering the expressions of the total energy of the H_{eff} of PMN are initially determined by conducting first-principles computations [43–45] on small cells. However, these parameters are also allowed to vary from their first-principles values in the present work, in order to obtain a better agreement with experiments. In particular and as discussed below, we found that two types of these parameters play an important role on properties of PMN and need to be carefully adjusted from their computed values. They are (i) the short-range parameter called j_5 in Ref. [36], that characterizes a specific interaction between second-nearest neighbors (e.g., between different Cartesian components of the local modes that are centered on two Pb sites that are the closest along the ⟨110⟩ pseudocubic directions); and (ii) the magnitude of the coefficients denoted by $Q_{|j-i|}(\sigma_j)$, which represent the strength and direction of the so-called random electric fields [12,24,46,47].

III. RESULTS AND DISCUSSIONS

Figure 1(a) reports the dielectric susceptibility χ of disordered PMN as a function of temperature, computed from the cumulant method detailed in Ref. [48] and involving the local soft modes (χ therefore corresponds to the experimental situation for which *small* electric fields are applied). The dielectric susceptibility of PMN has a rounded peak while, as shown in the right inset of Fig. 1(b), no polarization is numerically found to appear on zero-field cooling, even at the lowest temperatures. Such features are consistent with experiments on PMN and are characteristics of relaxor ferroelectrics [3–5]. They also contrast with the case of "normal" ferroelectrics for which the dielectric susceptibility has a sharp peak around the paraelectric-to-ferroelectric phase transition temperature. Other information revealed by Fig. 1(a) is that χ follows a Curie-Weiss law [49] $C/(T - T_0)$ (where T is the temperature, and with $C = 1.27 \times 10^5$ K and $T_0 = 400$ K) for temperatures above $\simeq$600 K, while it deviates from this law for temperatures below 600 K. Interestingly, this latter temperature corresponds to the Burns temperature ($T_B = 620$ K) reported for PMN [6] below which there is a known deviation of χ from the Curie-Weiss law, and above which the Curie-Weiss law is well obeyed with $C = 1.25 \times 10^5$ K and $T_0 = 396$ K according to Ref. [5] (note that similar values of the Curie-Weiss constant were obtained in other experiments, e.g., $C = 2.05 \times 10^5$ K and $C \approx 10^5$ K in Refs. [11] and [14], respectively). Comparisons between the predicted and measured values of both T_B and T_0, as well as of the Curie-Weiss constant, therefore attest to the accuracy of the simulations after careful selection of the effective Hamiltonian parameters. It is also worth mentioning that χ exhibits rather large error bars for temperatures below T_B, in general, and close to or below its peak, in particular. This indicates that properties of PMN are rather sensitive to the atomic configuration. Moreover, T_0, which usually corresponds to the Curie temperature in normal ferroelectrics, can be identified here as the so-called T^* temperature inherent to relaxors [5,8,50–53]. We will come back to these points later on.

We also conducted simulations for which disordered PMN is cooled down under a dc electric field that is oriented along the pseudocubic [111] direction, and having Cartesian components equal to 1.0×10^7 V/m along the x, y, and z axes (the magnitude of this field is therefore $\sqrt{3} \times 10^7$ V/m). Under these circumstances, PMN adopts a significant electrical polarization along the direction of the applied field below a certain temperature, and, correspondingly, a large dc susceptibility (not shown here), which differs from the susceptibility, obtained by the cumulant method, and that can be considered as one of the main features of the relaxors and glasses [26]. Interestingly, such polarization remains finite when this field is removed at low temperature. The left inset of Fig. 1(b) reveals that this polarized state (obtained at 10 K here) possesses some degrees of disorder in it since not all the dipoles are aligned along the [111] direction—which is in contrast with the case of a typical ferroelectric like $BaTiO_3$ but is consistent with what was observed experimentally in PMN by local probes such as the nuclear magnetic resonance technique in Ref. [7]. We numerically find that this degree of disorder originates from the random electric fields existing inside PMN. The system is then heated *under no electric field* starting from this low-temperature, polarized state. The resulting temperature dependence of the Cartesian components of the supercell average of the local mode, $\langle \mathbf{u} \rangle$, is displayed in Fig. 1(b) (note that the x, y, and z axes are chosen along the pseudocubic [100], [010], and [001] directions, respectively). One can, e.g., see that the x, y, and z Cartesian components of $\langle \mathbf{u} \rangle$ are all predicted to have a magnitude of 0.050 a.u. at 10 K, 0.045 a.u. at 150 K, and of 0.039 at 250 K, which corresponds to a polarization of 0.54, 0.49, and 0.43 C/m^2, respectively, that is oriented along [111]. These magnitudes agree rather well with measurements providing 0.46 C/m^2 at

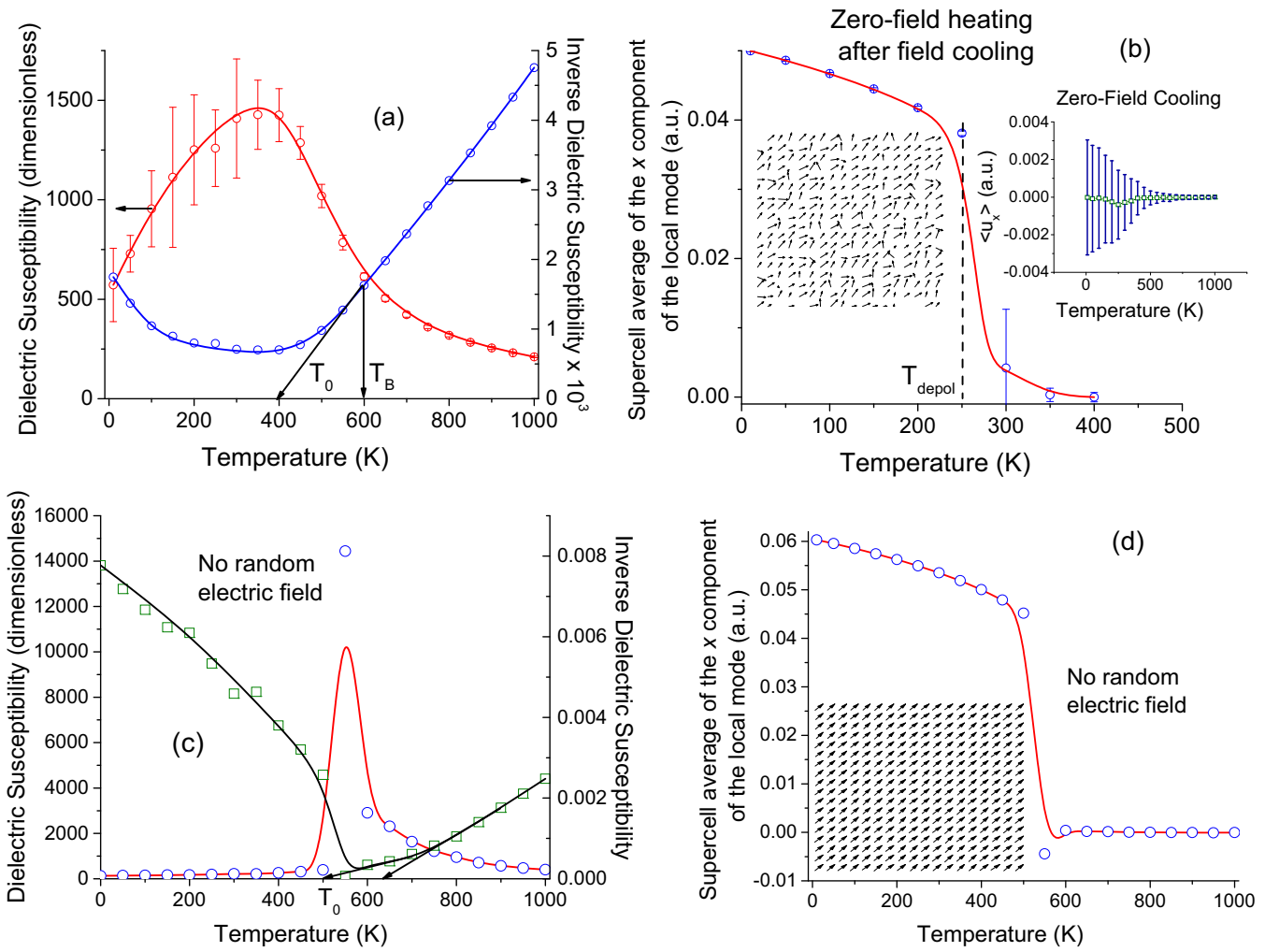

FIG. 1. (Color online) Predicted temperature dependence of several properties in PMN solid solutions. Panel (a) shows the dielectric susceptibility, and its inverse, when cooling down the disordered PMN system under no bias field. T_B and T_0 correspond to the Burns temperature and the critical temperature extrapolated from the Curie-Weiss law at high temperatures, respectively. Panel (b) displays the x component of the supercell average of the local mode, $\langle \mathbf{u} \rangle$, (which is equal to its y and z components) when heating the system is under no field, after having cooled it under an electric field and then having removed this field at 10 K. The depolarizing temperature is $T_{\rm depol} = 250 \pm 50$ K and is indicated by a vertical dashed line. The left inset of panel (b) shows an example of the dipolar configuration when the field is removed at 10 K. The right inset of panel (b) shows the x component of $\langle \mathbf{u} \rangle$, but when the system is cooled under no field. The error bars in panels (a) and (b) are those arising from computing averages over 30 different chemical configurations. Panels (c) and (d) show the dielectric susceptibility (as well as its inverse) and the x component of the supercell average of the local mode (which is identical to its y and z components), respectively, when random fields are switched off. The left inset of panel (d) displays the resulting dipolar configuration at 10 K, when random fields are turned off.

temperature close to 0 K [54] and 0.41 C/m^2 at 150 K [55] as well as with first-principles calculations yielding values ranging between 0.40 and 0.65 C/m^2 at 0 K [38,39]—which further emphasizes the capability of our $H_{\rm eff}$ to realistically mimic the complex properties of PMN. Figure 1(b) also indicates that the polarization decreases on heating and then, at about 250 ± 50 K, experiences a sudden jump down leading to its vanishing. Such striking behavior has indeed been experimentally reported, with the temperature associated with this jump being called the depolarization temperature $T_{\rm depol}$, and being equal to $\simeq$210–230 K for (111) crystals [12,56–58]. The temperature at which this jump occurs is also linked to the freezing temperature T_f, below which PMN is nonergodic [12]—as evidenced in Fig. 1(b) by the different ground states obtained depending on the cooling regime (zero-field cooling or removing of electric field after field cooling).

Having demonstrated the predictive capability of our simulations at both global/macroscopic [cf. Fig. 1(a)] and local/nanoscopic [left inset of Fig. 1(b)] levels, let us now provide a microscopic insight of PMN by showing, in Figs. 2(a)–2(d), snapshots of the dipolar patterns within a (x, y) plane for different temperatures, when the system is cooled under no field. These snapshots reveal that correlated clusters, usually referred to as polar nanoregions (PNRs) and inside which dipoles are nearly parallel to each other and contain at least two Pb-centered dipoles, indeed exist in PMN, as suggested in Refs. [6,40,58–61] and similar to the case of the homovalent BZT relaxor [23,42,62,63]. These PNRs are

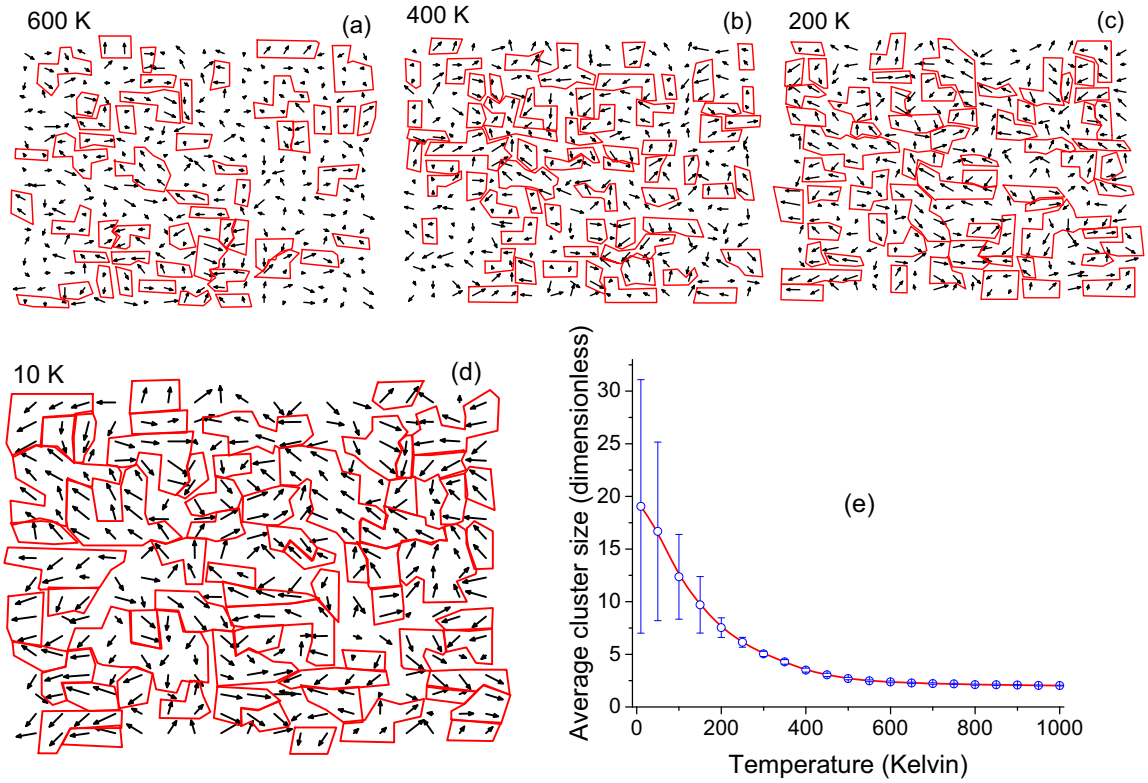

FIG. 2. (Color online) Snapshots of the local modes' patterns within a (x, y) plane for different temperatures, panels (a)–(d), and temperature dependence of the average size of the polar nanoregions, panel (e), when disordered PMN is cooled under no field. In panels (a)–(d), the corresponding temperature is indicated on the top left and the red lines delimit the PNRs. The error bars in panel (e) are those resulting from incorporating 30 different chemical configurations into the computation of the averaged PNR size.

delimited by red lines in Figs. 2(a)–2(d), and are numerically found by using the same Bayesian algorithm as in Refs. [42,62] from instantaneous snapshots (configuration of the last Monte Carlo sweep for any investigated temperature). Their average (dimensionless) size [64] is computed as $\langle s\rangle = \langle N^2\rangle/\langle N\rangle$, where N is the number of Pb sites belonging to a PNR, and the brackets denote the average over all the PNRs existing inside the supercell. Figure 2(e) displays the predicted temperature dependency of $\langle s\rangle$. The data of Fig. 2 indicate that $\langle s\rangle$ rapidly grows and the number of PNRs becomes larger upon cooling below T_B, in general, and below T_f, in particular (note that PNRs containing a single Pb dipole are included in the definition of $\langle s\rangle$, which explains why $\langle s\rangle$ is not equal to 0 above the Burns temperature). Indeed, Figs. 2(c) and 2(d) reveal the large number of PNRs below 200 K, and Fig. 2(e) demonstrates an average cluster size of 19. Interestingly, such size corresponds, in one dimension, to a length of about 72 Å, which is similar to the spatial correlation length of 62.4 Å obtained experimentally by neutron diffuse scattering [58] at 10 K. Note that the Supplemental Material also discusses the dynamic versus static characters of these PNRs for different temperatures (see Fig. 1 there), which is found to be in line with experimental findings [51,58]. As a result, on decreasing temperature, the size (cf. Fig. 2) and the degree of the static character (see the Supplemental Material [30]) of the polar correlations in PMN are increasing to get a microscopic configuration, below T_f, which is described by many nanosize clusters that are separated from a few isolated, nonvanishing dipoles, or that can even touch each other—which contrast with the case of BZT [23].

Let us now discuss and reveal the key features at the origin of the aforementioned microscopic description and properties of PMN relaxor. For that, we first decided to compute correlations between dipoles as follows:

$$\theta_{\alpha,\alpha}(\mathbf{r}) = \frac{1}{N_{sc}}\sum_i \frac{u_{i,\alpha}u_{i+r,\alpha}}{|\mathbf{u_i}\cdot\mathbf{u_{i+r}}|}, \qquad (1)$$

where the index i runs over all the N_{sc} Pb sites of the supercell and where $\mathbf{u_i}$ and $\mathbf{u_{i+r}}$ are the local modes in cell i and in the cell centered on the Pb atom distant from $\mathbf{r}$ from the cell i, respectively [65]. $u_{i,\alpha}$ and $u_{i+r,\alpha}$ are the α-Cartesian components of $\mathbf{u_i}$ and $\mathbf{u_{i+r}}$, respectively. Note that $\theta_{\alpha,\alpha}(\mathbf{r})$ is equal to 1/3 for any α (i.e., x, y or z) and for any $\mathbf{r}$ in the hypothetical case for which the dipoles all have the same magnitude and are all lying along the pseudocubic [111] direction. Positive and negative signs of $\theta_{\alpha,\alpha}(\mathbf{r})$ are representative of correlations and anticorrelations, respectively, between the α component of $\mathbf{u_i}$ and $\mathbf{u_{i+r}}$. Figures 3(a) and 3(b) display $\theta_{x,x}(\mathbf{r})$ for the $\mathbf{r}$ vectors lying in the (x, y) plane, at 10 K and for two different realizations of disordered PMN. While these two correlations between the x components of the local modes can present some differences in, e.g., shape, anisotropy, and values at some particular $\mathbf{r}$ distances, they also share a remarkable feature: the existence of significant *anticorrelations* in regions of space centered about $\mathbf{r_1} = \pm 4.5a_{\text{lat}}\mathbf{x}$ and $\mathbf{r_2} = \pm 4.5a_{\text{lat}}\mathbf{x} \pm 9a_{\text{lat}}\mathbf{y}$ in our $18 \times 18 \times 18$ supercell, where a_{lat} is the lattice constant

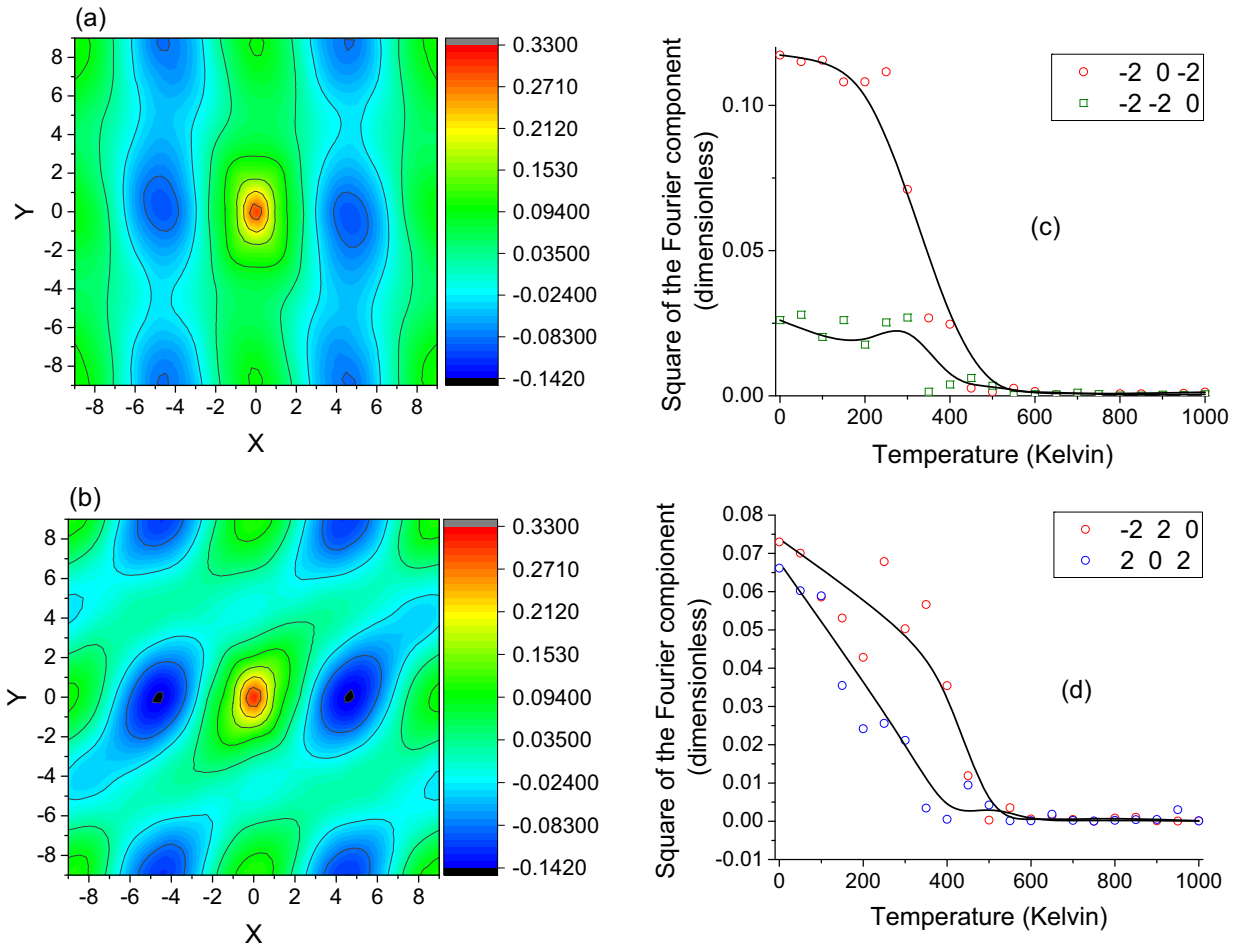

FIG. 3. (Color online) Properties associated with anticorrelations and off-center points in disordered PMN. Panels (a) and (b) show the $\theta_{x,x}(\mathbf{r})$ correlation between the x components of the local modes centered on lead atoms for the $\mathbf{r}$ vectors ling in the (x,y) plane at 10 K for two different realizations of the disordered PMN system. Panels (c) and (d) display the temperature dependence of the square of the Fourier transform of the x component of the local modes' configurations for different $\mathbf{k}_{\max,i}$ points for the atomic configurations corresponding to panels (a) and (b), respectively. The three integers n_x, n_y, and n_z indicated in the legends of panels (c) and (d) index the $\mathbf{k}_{\max,i}$ points, that is such k points are given by $\frac{2\pi}{18a_{\rm lat}}(n_x\mathbf{x}+n_y\mathbf{y}+n_z\mathbf{z})$ for our $18\times18\times18$ supercell. Note also that the square of the Fourier transform of the x component of the local modes' configurations is invariant by inversion in the reciprocal space, i.e., $\frac{2\pi}{18a_{\rm lat}}(n_x\mathbf{x}+n_y\mathbf{y}+n_z\mathbf{z})$ and $\frac{2\pi}{18a_{\rm lat}}(-n_x\mathbf{x}-n_y\mathbf{y}-n_z\mathbf{z})$ have precisely the same value of the Fourier transform.

of the five-atom primitive cell and where $\mathbf{x}$ and $\mathbf{y}$ are unit vectors along the x and y axis, respectively. Note that we also numerically found (not shown here) (1) similar anticorrelations of the x components of the local modes in the (x,z) plane for regions centered about $\mathbf{r_1}$ and $\mathbf{r_3}=\pm4.5a_{\rm lat}\mathbf{x}\pm9a_{\rm lat}\mathbf{z}$ (where $\mathbf{z}$ is the unit vector along the z axis); and (2) similar anticorrelations of the y and z components of the local modes in the planes and around positions that can be deduced by cyclic permutations from the case of the anticorrelations between the x components of the local modes. These anticorrelations can be thought of as representative of antiferroelectriclike interactions existing inside PMN, which is consistent with the previously suggested idea that antiferroelectricity plays some role in relaxor behaviors [22,23,66–69]. Moreover, such anticorrelations between the x components of the local modes were further found to be associated with the Fourier transform of the distribution of the x component of the local modes inside the supercell [70] being significant at *several off-center vectors* of the first Brillouin zone. Typically, in our $18\times18\times18$ supercells, these off-center k points are among the eight given by $\frac{2\pi}{9a_{\rm lat}}(\pm\mathbf{x}\pm\mathbf{y})$ and $\frac{2\pi}{9a_{\rm lat}}(\pm\mathbf{x}\pm\mathbf{z})$, and that will be denoted as $\mathbf{k}_{\max,i}$ in the following, where i runs from 1 to 8. Note that (1) for the case of the x components of the local modes, these $\mathbf{k}_{\max,i}$ lie, close to Γ, along the $\Gamma-M$ lines of the first Brillouin zone, where the M points are given by $\frac{\pi}{a_{\rm lat}}(\pm\mathbf{x}\pm\mathbf{y})$; (2) the $\mathbf{k}_{\max,i}$ are given by $\frac{2\pi}{9a_{\rm lat}}(\pm\mathbf{x}\pm\mathbf{y})$ and $\frac{2\pi}{9a_{\rm lat}}(\pm\mathbf{y}\pm\mathbf{z})$ for the Fourier transform of the *y components* of the local modes, and by $\frac{2\pi}{9a_{\rm lat}}(\pm\mathbf{x}\pm\mathbf{z})$ and $\frac{2\pi}{9a_{\rm lat}}(\pm\mathbf{y}\pm\mathbf{z})$ for the Fourier transform of the *z components* of the local modes; and (3) the $\mathbf{k}_{\max,i}$ vectors also depend on the size of the periodic supercell used in the simulations. For instance, they are still lying along the $\Gamma-M$ lines of the first Brillouin zone when using $N\times N\times N$ supercells with $N=12$, 14, or 16, but their magnitude is now equal to $\sqrt{2}\frac{2\pi}{Na_{\rm lat}}$ in these cases (note that these k points are thus not located at zone *boundaries*). As a result, one can infer that the magnitude of the "real" $\mathbf{k}_{\max,i}$ for which the Fourier

transforms of the Cartesian components of the local modes are maximum ranges 0.0884–0.1571 in $\frac{2\pi}{a_{\text{lat}}}$ units (note that this magnitude can also be rather sensitive to the j_5 parameter).

Furthermore, Figs. 3(c) and 3(d) display the temperature evolution of the square of the Fourier transform of the x component of the local dipoles configuration at some of these $\mathbf{k}_{\text{max},i}$ points for the two alloy configurations associated with Figs. 3(a) and 3(b), respectively. Interestingly, these quantities are nonzero only below 450 ± 50 K, which we identify as the so-called T^* critical temperature of relaxors and which we also considered to be equal to T_0 in the aforementioned Curie-Weiss relationship for the dielectric response. Note that different measurements provide values of 350 K [50], 400 K [5,8,51], and 500 K [52] for T^* in PMN, and that both hyper-Raman [71] and inelastic neutron [72] scattering techniques pointed out to a condensation of the soft polar mode at respectively 400 and 340-K. It is interesting to realize that the onset of anticorrelations shown in Figs. 3(c) and 3(d) occurs in a temperature range that is consistent with the condensation of the M- and R-point zone boundary soft modes observed in PMN by Swainson *et al.* [69] between 400 and 450 K. Such experimental data (i) therefore cover a rather wide temperature interval inside which our prediction falls in and (ii) which can be understood by realizing that Figs. 3(c) and 3(d) reveal that this T^* can depend on the alloy configuration (and thus should be experimentally dependent on the sample preparation and the spatial (and probably time) scale resolution of the experimental technique). As a matter of fact, Fig. 3(c) gives a T^* close to 400 K while Fig. 3(d) yields a value closer to 450 K. Note that the Supplemental Material also provides additional details about the effect of atomic ordering on properties of PMN systems. Figures 3(c) and 3(d) further show that the square of the Fourier transform increases when decreasing the temperature below T^* until reaching a rather significant value that also strongly depends on the atomic configuration used to represent disordered PMN. For instance, the two configurations resulting in the correlations depicted in Figs. 3(a)and 3(b) possess values of about 12% for $\frac{2\pi}{9a_{\text{lat}}}(\mathbf{x}+\mathbf{z})$ and of about 7% for $\frac{2\pi}{9a_{\text{lat}}}(\mathbf{x}+\mathbf{y})$ of the total spectra gathering the Fourier transforms at all possible k points at 10 K, respectively. Such results indicate that, as similar to the BZT case [23], anticorrelations begin to occur at the T^* critical temperature and strengthen as the temperature is reduced below T^*. The fact that Figs. 3(c) and 3(d) demonstrate that *several* of these symmetry-related $\mathbf{k}_{\text{max},i}$ exist for any disordered atomic configuration at any temperature below T^* makes the disordered PMN different from an incommensurate crystal, for which only a *single* off-center k point condenses at a critical temperature in one macroscopic domain [15,73]. The simultaneous condensation of several k points presently discovered here is also a key ingredient of the so-called weak crystallization theory [74] and is also likely consistent with the idea of phonon localization advanced in Refs. [75,76] to explain the relaxor behavior in PMN (note also that the occurrence of correlated regions localized in real space, such as the PNRs, also automatically imply the existence of more than one k point in the Fourier transform of the local modes). It is important to know that increasing the magnitude of a specific short-range order parameter between second nearest neighbors (namely, the j_5 coefficient indicated in the methods section) was numerically found to enhance both the strengths of the anticorrelations and of the Fourier transform of the local modes at $\mathbf{k}_{\text{max},i}$ for any temperature below T^*, therefore demonstrating its relevance to understand PMN, as well as the possibility for tuning relaxorlike properties.

Interestingly, we can also infer that, in addition to j_5, the random electric fields are also key ingredients at the very heart of the properties of PMN. To illustrate this fact, we conducted additional simulations in which the random electric fields are switched off [practically, the $Q_{|j-i|}(\sigma_j)$ coefficients are imposed to be null]. Figures 1(c) and 1(d) show the resulting temperature dependency of the dielectric response and of the x component of the $\langle \mathbf{u} \rangle$ supercell average of the local modes (which is also equal to its y and z components), respectively, when the system is progressively cooled from high temperature down to 10 K. Comparing Fig. 1(a) with Figs. 1(c) and 1(d) tells us that the random electric fields play a primordial role in the relaxor behavior of PMN: without them, disordered PMN would display a first-order transition at around 550 ± 50 K (that is characterized by a large and sharp peak in the dielectric susceptibility) above which the system is macroscopically paraelectric while below which it is ferroelectric with an electrical polarization lying along the pseudocubic [111] direction and increasing in magnitude as the temperature is reduced [as shown by Fig. 1(d)]. Figure 1(c) further shows that the Curie-Weiss law is also followed for temperatures above 750 K with a corresponding T_0 of 633 K, when random fields are not included in the simulations. Surprisingly, for temperatures ranging $T = 550$ to 750 K (that is "just" above the transition temperature) another Curie-Weiss law is obeyed, one for which T_0 is now very close to 500 K. We numerically find that the existence of these two different Curie-Weiss laws originates from the appearance of the aforementioned (j_5-driven) antiferroelectric (AFE) -like features for temperatures ranging 550–750 K. On the other hand, these AFE-like features are found to vanish in favor of a ferroelectric state for temperatures smaller than 550 ± 50 K, that is below the phase transition—as demonstrated by the inset of Fig. 1(d) revealing that the low-temperature polar state is homogeneous, when random electric fields are turned off. Such findings therefore demonstrate the strong competition between ferroelectric and AFE-like interactions. Moreover, It is also important to know that the temperature at which the peak of the dielectric response occurs when random fields are neglected does *not* necessarily coincide with the Burns temperature nor T_0 or T^* of the true disordered PMN system [i.e., incorporating the $Q_{|j-i|}(\sigma_j)$ coefficients]. As a matter of fact, we numerically found that it is possible to find *different* combinations between the aforementioned j_5 and $Q_{|j-i|}(\sigma_j)$ parameters giving the same T_0 and T_B as in Fig. 1(a) for disordered PMN [in general the larger j_5 is in magnitude the bigger $Q_{|j-i|}(\sigma_j)$ is for these combinations], while the position of the peak of the dielectric response reported in Fig. 1(c) (in the case of no random electric field) does depend on this combination. Note that, technically speaking, we also needed to vary a third effective Hamiltonian parameter, along with j_5 and $Q_{|j-i|}(\sigma_j)$ coefficients, to have a fixed T_0 temperature. This third parameter is the harmonic coefficient of the local electric dipoles, and is therefore directly related to the strength of the ferroelectric instability at the zone center. Such facts

(further) demonstrate that ferroelectric degrees of freedom, antiferroelectriclike motions, and random fields all interact with each other to produce the striking properties of disordered PMN, and thus all need to be accounted for to understand this complex system, in particular, and lead-based relaxors, in general.

IV. SUMMARY

In summary, we develop and use an effective Hamiltonian method to study finite-temperature properties of PMN. This numerical technique reproduces known anomalous striking signatures of this prototype of relaxor ferroelectrics, therefore demonstrating its accuracy and capability. It also reveals the nanoscale picture of PMN and the microscopic origins of its properties. It is also worth realizing that a similar technique was recently used to investigate the lead-free and homovalent $Ba(Zr,Ti)O_3$ system [23]. Comparing that study [23] to the present one reveals that different relaxor ferroelectrics can exhibit similar macroscopic properties but their microscopic origins can be fundamentally different: in one case, the difference in polarizability between the ions belonging to the mixed sublattice [that is Ti and Zr in $Ba(Zr,Ti)O_3$] was found to be essential to reproduce relaxor behavior via the formation of small embedded polar nanoregions. On the other hand, in the case of PMN, the major players are the random electric fields arising from the mixed B sublattice, the strong short-range interactions between lead-centered electrical dipoles, and the competition between ferroelectric and antiferroelectric interactions, which result in a complex nanodomain structure exhibiting anticorrelations associated with several off-center k points. We therefore hope that the present work results in a deeper and broader knowledge of the fascinating class of relaxor ferroelectrics, and can also be useful for the understanding of other inhomogeneous systems with remarkable properties like colossal magnetoresistance or high-temperature superconductivity where competing states in the presence of random fields are key ingredients too [77].

ACKNOWLEDGMENTS

This work was financially supported by Grant No. N00014-12-1-1034 (S.P. and L.B.) and NSF Grant No. DMR-1066158 (D.W.). D.W. also acknowledges support from National Natural Science Foundation of China (Grant No. 51390472) and National Basic Research Program of China (Grant No. 2015CB654903).

[1] T. Kimura, Y. Tomioka, R. Kumai, Y. Okimoto, and Y. Tokura, Phys. Rev. Lett. **83**, 3940 (1999).
[2] V. V. Laguta, V. A. Stephanovich, M. Savinov, M. Marysko, R. O. Kuzian, I. V. Kondakova, N. M. Olekhnovich, A. V. Pushkarev, Yu. V. Radyush, I. P. Raevski, S. I. Raevskaya, and S. A. Prosandeev, New J. Phys. **16**, 113041 (2014).
[3] L. E. Cross, Ferroelectrics **151**, 305 (1994).
[4] G. A. Smolensky *et al.*, *Ferroelectrics and Related Materials* (Gordon and Breach, New York, 1981).
[5] D. Viehland, S. J. Jang, L. E. Cross, and M. Wuttig, J. Appl. Phys. **68**, 2916 (1990).
[6] G. Burns and F. H. Dacol, Phys. Rev. B **28**, 2527 (1983).
[7] R. Blinc, V. V. Laguta, and B. Zalar, Phys. Rev. Lett. **91**, 247601 (2003).
[8] B. Dkhil, J. M. Kiat, G. Calvarin, G. Baldinozzi, S. B. Vakhrushev, and E. Suard, Phys. Rev. B **65**, 024104 (2001).
[9] P. M. Gehring, S. Wakimoto, Z.-G. Ye, and G. Shirane, Phys. Rev. Lett. **87**, 277601 (2001).
[10] A. K. Tagantsev and A. E. Glazounov, Phys. Rev. B **57**, 18 (1998).
[11] D. Fu, H. Taniguchi, M. Itoh, S.-ya Koshihara, N. Yamamoto, and S. Mori, Phys. Rev. Lett. **103**, 207601 (2009).
[12] V. Westphal, W. Kleemann, and M. D. Glinchuk, Phys. Rev. Lett. **68**, 847 (1992).
[13] J. Hlinka, J. Adv. Dielectr. **2**, 1241006 (2012).
[14] A. A. Bokov and Z.-G. Ye, J. Mater. Sci. **41**, 31 (2006).
[15] R. A. Cowley, S. N. Gvasaliya, S. G. Lushnikov, B. Roessli, and G. M. Rotaru, Adv. Phys. **60**, 229 (2011).
[16] P. K. Davies and M. A. Akbas, J. Phys. Chem. Solids **61**, 159 (2000).
[17] P. Ganesh, E. Cockayne, M. Ahart, R. E. Cohen, B. Burton, Russell J. Hemley, Yang Ren, Wenge Yang, and Z.-G. Ye, Phys. Rev. B **81**, 144102 (2010).
[18] S. Tinte, B. P. Burton, E. Cockayne, and U. V. Waghmare, Phys. Rev. Lett. **97**, 137601 (2006).
[19] I. Grinberg, P. Juhás, P. K. Davies, and A. M. Rappe, Phys. Rev. Lett. **99**, 267603 (2007).
[20] V. S. Vikhnin, S. E. Kapphan, I. L. Kislova, R. I. Eglitis and P. A. Markovin, Ferroelectrics **285**, 291 (2003).
[21] R. F. Mamin and R. Blinc, Phys. Solid State **45**, 942 (2003).
[22] V. M. Ishchuk, V. N. Baumer, and V. L. Sobolev, J. Phys.: Condens. Matter **17**, L177 (2005).
[23] A. R. Akbarzadeh, S. Prosandeev, E. J. Walter, A. Al-Barakaty, and L. Bellaiche, Phys. Rev. Lett. **108**, 257601 (2012).
[24] B. E. Vugmeister and M. D. Glinchuk, Rev. Mod. Phys. **62**, 993 (1990).
[25] R. Pirc and R. Blinc, Phys. Rev. B **60**, 13470 (1999).
[26] D. Sherrington, Phys. Rev. Lett. **111**, 227601 (2013); Phys. Rev. B **89**, 064105 (2014).
[27] G. G. Guzmán-Verri, P. B. Littlewood, and C. M. Varma, Phys. Rev. B **88**, 134106 (2013).
[28] I.-K. Jeong, T. W. Darling, J. K. Lee, Th. Proffen, R. H. Heffner, J. S. Park, K. S. Hong, W. Dmowski, and T. Egami, Phys. Rev. Lett. **94**, 147602 (2005).
[29] W. Dmowski, S. B. Vakhrushev, I.-K. Jeong, M. P. Hehlen, F. Trouw, and T. Egami, Phys. Rev. Lett. **100**, 137602 (2008).
[30] See Supplemental Material at http://link.aps.org/supplemental/10.1103/PhysRevB.91.214117 for detailed information about the effective Hamiltonian scheme used here, and also results related to the static versus dynamical character of the PNRs and the influence of chemical ordering on properties of $PbMg_{1/3}Nb_{2/3}O_3$ systems.
[31] A. L. Roytburd, Phase Transit. **45**, 1 (1993).
[32] R. Hemphill, L. Bellaiche, A. Garcia, and D. Vanderbilt, Appl. Phys. Lett. **77**, 3642 (2000).
[33] O. Bidault, C. Perrin, C. Caranoni, and N. Menguy, J. Appl. Phys. **90**, 4115 (2001); C. Perrin, N. Menguy, O. Bidault, C. Y.

Zahra, A.-M. Zahra, C. Caranoni, B. Hilczer, and A. Stepanov, J. Phys.: Condens. Matter **13**, 10231 (2001).
[34] N. Setter and L. E. J. Cross, Appl. Phys. **51**, 4356 (1980).
[35] C. Malibert, B. Dkhil, J. M. Kiat, D. Durand, J. F. Bérar, and A. Spasojevic-de Biré, J. Phys.: Condens. Matter **9**, 7485 (1997).
[36] W. Zhong, D. Vanderbilt, and K. M. Rabe, Phys. Rev. B **52**, 6301 (1995); Phys. Rev. Lett. **73**, 1861 (1994).
[37] S. Vakhrushev, S. Zhukov, G. Fetisov, and V. Chernyshov, J. Phys.: Condens. Matter **6**, 4021 (1994).
[38] N. Choudhury, Z. Wu, E. J. Walter, and R. E. Cohen, Phys. Rev. B **71**, 125134 (2005).
[39] S. A. Prosandeev, E. Cockayne, B. P. Burton, S. Kamba, J. Petzelt, Yu. Yuzyuk, R. S. Katiyar, and S. B. Vakhrushev, Phys. Rev. B **70**, 134110 (2004).
[40] A. Naberezhnov, S. Vakhrushev, B. Dorner, D. Strauch, and H. Moudden, Eur. Phys. J. B **11**, 13 (1999).
[41] L. Bellaiche, A. Garcia, and D. Vanderbilt, Phys. Rev. Lett. **84**, 5427 (2000); Ferroelectrics **266**, 41 (2002).
[42] S. Prosandeev, D. Wang, and L. Bellaiche, Phys. Rev. Lett. **111**, 247602 (2013).
[43] L. Bellaiche and D. Vanderbilt, Phys. Rev. B **61**, 7877 (2000).
[44] P. Hohenberg and W. Kohn, Phys. Rev. **136**, B864 (1964); W. Kohn and L. J. Sham, *ibid.* **140**, A1133 (1965).
[45] D. Vanderbilt, Phys. Rev. B **41**, 7892(R) (1990).
[46] J. Iñiguez and L. Bellaiche, Phys. Rev. B **73**, 144109 (2006).
[47] B. E. Vugmeister and H. Rabitz, Phys. Rev. B **57**, 7581 (1998).
[48] K. M. Rabe and E. Cokayne, *First-Principles Calculations for Ferroelectrics: Fifth Williamsburg Workshop*, edited by R. E. Cohen (AIP, Woodbury, NY, 1998), p. 61.
[49] F. Jona and G. Shirane, *Ferroelectric Crystals* (Dover, New York, 1993).
[50] O. Svitelskiy, J. Toulouse, G. Yong, and Z.-G. Ye, Phys. Rev. B **68**, 104107 (2003).
[51] C. Stock, L. Van Eijck, P. Fouquet, M. Maccarini, P. M. Gehring, G. Xu, H. Luo, X. Zhao, J.-F. Li, and D. Viehland, Phys. Rev. B **81**, 144127 (2010).
[52] B. Dkhil, P. Gemeiner, A. Al-Barakaty, L. Bellaiche, E. Dul'kin, E. Mojaev, and M. Roth, Phys. Rev. B **80**, 064103 (2009).
[53] S. Prosandeev, I. P. Raevski, M. A. Malitskaya, S. I. Raevskaya, H. Chen, C.-C. Chou, and B. Dkhil, J. Appl. Phys. **114**, 124103 (2013).
[54] Z.-G. Ye and H. Schmid, Ferroelectrics **145**, 83 (1993).
[55] R. Sommer, N. K. Yushin, and J. J. van der Klink, Phys. Rev. B **48**, 13230 (1993).
[56] E. V. Colla, E. Yu. Koroleva, N. M. Okuneva, and S. B. Vakhrushev, Ferroelectrics **184**, 209 (1996).
[57] R. Pirc, Z. Kutnjak, and N. Novak, J. Appl. Phys. **112**, 114122 (2012).
[58] G. Xu, G. Shirane, J. R. D. Copley, and P. M. Gehring, Phys. Rev. B **69**, 064112 (2004).
[59] S. B. Vakhrushev, B. E. Kvyatkovsky, A. A. Naberezhnov, N. M. Okuneva, and B. P. Toperverg, Ferroelectrics **90**, 173 (1989).
[60] K. Hirota, Z.-G. Ye, S. Wakimoto, P. M. Gehring, and G. Shirane, Phys. Rev. B **65**, 104105 (2002).
[61] S. Vakhrushev, A. Nabereznov, S. K. Sinha, Y. P. Feng, and T. Egami, J. Phys. Chem. Solids **57**, 1517 (1996).
[62] S. Prosandeev, D. Wang, A. R. Akbarzadeh, B. Dkhil, and L. Bellaiche, Phys. Rev. Lett. **110**, 207601 (2013).
[63] D. Wang, J. Hlinka, A. A. Bokov, Z.-G. Ye, P. Ondrejkovic, J. Petzelt, and L. Bellaiche, Nat. Commun. **5**, 5100 (2014).
[64] D. Stauffer and A. Aharony, *Introduction to Percolation Theory* (Taylor & Francis, London, 1994).
[65] A. R. Akbarzadeh, L. Bellaiche, K. Leung, J. Íñiguez, and D. Vanderbilt, Phys. Rev. B **70**, 054103 (2004).
[66] N. Takesue, Y. Fujii, M. Ichihara, and H. Chen, Phys. Rev. Lett. **82**, 3709 (1999).
[67] W. Hu, K. Hayashi, K. Ohwada, J. Chen, N. Happo, S. Hosokawa, M. Takahasi, A. A. Bokov, and Z.-G. Ye, Phys. Rev. B **89**, 140103(R) (2014).
[68] A. Tkachuk and C. Chen, arXiv:cond-mat/0303105.
[69] I. P. Swainson, C. Stock, P. M. Gehring, Guangyong Xu, K. Hirota, Y. Qiu, H. Luo, X. Zhao, J.-F. Li, and D. Viehland, Phys. Rev. B **79**, 224301 (2009).
[70] A. M. George, J. Íñiguez, and L. Bellaiche, Phys. Rev. B **65**, 180301(R) (2002).
[71] A. Al-Zein, J. Hlinka, J. Rouquette, and B. Hehlen, Phys. Rev. Lett. **105**, 017601 (2010).
[72] S. B. Vakhrushev and S. M. Shapiro, Phys. Rev. B **66**, 214101 (2002).
[73] *Incommensurate Phases in Dielectrics*, edited by R. Blinc and A. P. Levanyuk (North-Holland, Amsterdam, 1986), Vols. 1 and 2.
[74] E. I. Kats, V. V. Lebedev, and A. R. Muratov, Phys. Rep. **228**, 1 (1993).
[75] A. Bussmann-Holder, J. Phys.: Condens. Matter **24**, 273202 (2012).
[76] M. E. Manley, J. W. Lynn, D. L. Abernathy, E. D. Specht, O. Delaire, A. R. Bishop, R. Sahul, and J. D. Budai, Nat. Commun. **5**, 3683 (2014).
[77] E. Dagotto, Science **309**, 257 (2005).